ILASS 2008
Sep. 8-10, 2008, Como Lake, Italy

Paper ID ILASS08-13-6

CAPILLARY FLOW OF LIQUID UNDER DROPLET IMPACT CONDITIONS

Vladimir Kogan, Eric Johnson, Phil Schumacher, and Brent Shroy

Battelle Memorial Institute
505 King Ave., Columbus, OH 43201, USA

ABSTRACT

Experimental studies and model calculations were performed investigating the capillary flow of viscous liquid caused by droplet impact on a porous surface. A series of experiments was conducted in which the dynamics of capillary flow was monitored under the conditions of single droplet impact on a transparent block containing a single capillary. Capillaries having 0.1, 0.3, and 0.5 mm in diameter were used in this work; droplets were generated using DI water and a 0.1 percent solution of Triton X-100 surfactant as the test liquids. The liquid penetration depth into the capillary and spread radius on the surface of the block were recorded using a high speed video system. The capillary flow dynamics was also modeled using the Bosanquet capillary flow equation, which was modified to account for the highly transient behavior of the droplet impact event, in which the impact pressure is a rapidly decaying function of time. Comparison between model predictions and experimental observations showed a notable consistency with regard to the capillary penetration distance as a function of time.

INTRODUCTION

Permeation of liquid into porous materials is a process that plays essential roles in many industrial applications, such as civil engineering, oil recovery, printing, agriculture, textile industry, etc. Because of the broad practical applications and scientific interests, this process has been extensively studied in the past, using both theoretical analyses and experimental techniques.

Considering a porous material as a matrix of sufficiently small capillaries, when a liquid is brought into contact with the surface of the material it spontaneously flows into the capillaries (provided that the liquid wets the material), driven by the difference between interfacial pressures of the liquid-solid and liquid-gas interfaces (i.e., by the capillary pressure). At equilibrium, the depth of liquid infiltration into the capillary is determined from the balance between the capillary pressure and the hydrostatic pressure of the liquid, which takes the following form for a vertical cylindrical capillary:

$$\frac{2\sigma\cos(\theta)}{r_c} = \rho g h_e \qquad (1)$$

In a number of practical applications, as well as from purely theoretical perspectives, it has been of interest to understand the dynamics of infiltration flow into porous materials, as a function of time. Some of the earlier findings related to the dynamics of capillary flow were accomplished by Lucas [1] and Washburn [2], who extended Eq. (1) to account for the viscous drag that develops during the flow of liquid in the capillary and obtained the following equation:

$$8\pi\mu z\frac{dz}{dt} = \frac{2\sigma\cos(\theta)}{r_c} - \rho g h_e \qquad (2)$$

Equation (2) describes a steady capillary flow, which was found to agree reasonably well with some experimental results in the asymptotic regimes of the process (e.g., [3]). However, one principal shortcoming of the Lucas-Washburn equation is that it does not account for the inertial effects associated with any transient flow, including the capillary flow of liquid caused by droplet impact on the surface of porous material. Bosanquet [4] modified the Lucas-Washburn equation by adding to it an inertial term, which resulted in the following equation of the dynamics of liquid capillary flow:

$$\underbrace{\frac{d}{dt}\left(\pi r_c^2 \rho z\frac{dz}{dt}\right)}_{\text{Inertial Loss}} + \underbrace{8\pi\mu z\frac{dz}{dt}}_{\text{Viscous Loss}} + \underbrace{\rho g z \pi r_c^2}_{\text{Gravitational Attraction}} = \underbrace{P_e\pi r_c^2}_{\text{Externally Applied Pressure}} + \underbrace{2\pi r_c\sigma\cos\theta}_{\text{Capillary Driving Force}} \qquad (3)$$

Equation (3) is a slightly modified version of the original Bosanquet equation, which is extended to include the effect of external pressure, P_e, if applied, acting on the liquid at the inlet of the capillary.

When liquid droplet impacts on the surface of porous material, a pressure pulse develops in the liquid, which serves as the primary driving force for both the spreading of the droplet on the surface and liquid permeation into the capillaries of the material. The capillary flow of viscous liquid

that develops due to droplet impact on the surface of porous material is investigated in this work.

THEORETICAL ANALYSIS

The dynamics of droplet impact on the surface containing a capillary is highly transient and complex. In the droplet impact process, two time-dependent and coupled processes take place: spreading of the droplet on the surface and flow of liquid into the capillary. These hydrodynamic processes develop over a very short amount time, on the order of milliseconds.

When liquid droplet impacts on the surface, a pulse of high pressure develops in the liquid within a time interval on the order of a few microseconds. Under this pressure, the liquid is driven to spread radially on the surface and is also forced to permeate into the capillaries of the porous material. This pressure pulse quickly dissipates due to viscous losses and surface evolution energy, and disappears at the end of the droplet spread process. The profile of the droplet impact pressure at the inlet point of the capillary that lasts during the droplet spread time is needed in order to solve the Bosanquet equation of the capillary flow, which requires knowing both the extent and the timeline of the droplet spreading process.

Several expressions have been proposed in the literature for the extent of the final spread radius of the droplet impacting a smooth surface, including Scheller and Bousfield [5], Toivakka [6], Mao et al. [7] and Pasandideh et al. [8]. Ukiwe et al. [9] performed an independent comparison of the Pasandideh's droplet final spread radius with experimental data and found a favorable agreement; Pasandideh's relationship includes the effects of the Reynolds number, the Weber number, and the liquid-surface contact angle as follows:

$$d_{sf} = d_0 \cdot \sqrt{\frac{We+12}{3\cdot(1-\cos(\theta))+4\cdot\left(\frac{We}{\sqrt{Re}}\right)}} \tag{4}$$

$$Re = \frac{\rho \cdot u \cdot d_0}{\mu}, \quad We = \frac{\rho \cdot u^2 \cdot d_0}{\sigma}$$

While Eq.(4) allows one to predict the final spread diameter of the droplet, it does not address the timescale over which the spreading occurs. In order to model the capillary flow of liquid due to droplet impact, the dynamics of the droplet spreading on the surface is important because it determines the time profile of the external pressure that controls the capillary penetration process. Pasandideh et al. [8] determined that the final droplet spread time can be estimated from the following equation:

$$t_{sf} = \frac{8}{3}\frac{d_0}{u} \tag{5}$$

Equations (4) and (5) allow for estimating the extent of droplet spreading on the surface and the time it takes to achieve the maximum spread, respectively. However, no reliable information was found in the literature regarding the time-dependent rate of droplet spreading over this final spread time. Therefore, a simple candidate correlation was proposed in this work to account for the dynamics of this spread process:

$$r_s(t) = r_{s0} + (r_{sf} - r_{s0}) \cdot (1 - e^{-kt}) \tag{6}$$

where k is a constant defined in a way that near the spread time t_{sf}, defined by Eq.(5), the spread radius r_s is approaching the final droplet spread radius r_{sf}:

$$k = \frac{-1}{t_{sf}} \cdot \ln\left[\frac{r_{sf}\cdot(1-X)}{r_{sf}-r_0}\right] \tag{7}$$

where X is the fraction of the final spread radius chosen to be reached by the final spread time t_{sf}, e.g., 0.99.

To implement Eq.(6), the initial droplet contact radius with the surface must also be estimated. Lubrication pressure at the final approach of the droplet will force the initial contact radius to be non-zero; therefore, a fraction of 0.5 of the initial spherical droplet radius was assumed for this analysis as a reasonable estimate of the initial contact radius. Note that a 500-μm water droplet traveling at terminal velocity (about 2 m/s) will have a final spread radius of about 1500 μm according to Eq.(4) and a final spread time of 0.7 ms according to Eq.(5).

As mentioned above, the pulse of pressure that develops inside the droplet when it impacts at sufficiently high velocity a surface containing a capillary will govern the initial rate of liquid flow into the capillary. It is reasonable to assume that the maximum pressure that is generated by the droplet impact event is proportional to the kinetic energy of the moving droplet. Correlation between the kinetic energy of a liquid slug impacting a solid surface and its impact pressure has been investigated in the past, e.g., by Chahine and Kalumuck [10]. In their work, comparison of the impact pressure with the stagnation pressure showed that the impact pressure was about 70% of the stagnation pressure. Therefore, for the purposes of this analysis, the maximum impact pressure is assumed to be:

$$P_0 = 0.7 \cdot \frac{\rho \cdot u^2}{2} \tag{8}$$

Consistent with the droplet spreading behavior, the impact-caused pressure profile also follows a dynamic process, changing in radial direction as well as with time. No reliable information was found in the literature specifically addressing the dynamics of pressure evolution upon droplet impact on the surface. Therefore, the following correlation was used in this work to describe the dynamics of the droplet impact pressure:

$$P(r,t) = P_0 \exp\left[-\left(\frac{\alpha \cdot r}{r_s(t)-r} + k \cdot t\right)\right] \tag{9}$$

where α is an empirical constant introduced for the impact pressure to dissipate everywhere when spread radius approaches its maximum value. Thus, according to Eq.(9), the droplet impact pressure on the surface approaches zero at the time-dependent spread radius as well as when spread time approaches t_{sf}. Figure 1 illustrates the shape of the pressure curves obtained using Eq.(9) for various times as a function of radius.

The dynamics of capillary flow driven by droplet impact on the surface is modeled using Equations (3) through (9) with initial conditions z_0=0.5r (a small initial penetration is required to avoid a nonphysical singularity in Eq.(3) at time

zero when a final force is applied to an infinitesimal mass of liquid in the capillary causing its infinite acceleration), and initial infiltration velocity varied at time zero from $dz/dt=0$ to $dz/dt=u$ (i.e., droplet impact velocity.

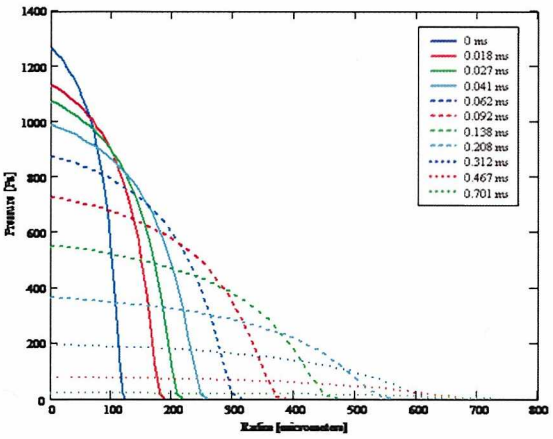

Figure 1. Droplet Impact Pressure Profile for a 500 μm Water Droplet at Terminal Velocity

The capillary flow equation, Eq.(3), which includes the effects of external pressure, capillary forces, gravity, and inertial and viscous losses, is a second order non-linear differential equation and must be solved numerically. The solution of this equation can be simplified by casting it into the form of two first order ordinary differential equations by introducing velocity as a second dependent variable.

EXPERIMENTAL STUDY

An experimental study was performed in which the effect of droplet impact velocity on the flow of liquid through a capillary was investigated. The study was performed using a falling droplet test apparatus a diagram of which is shown in Figure 2.

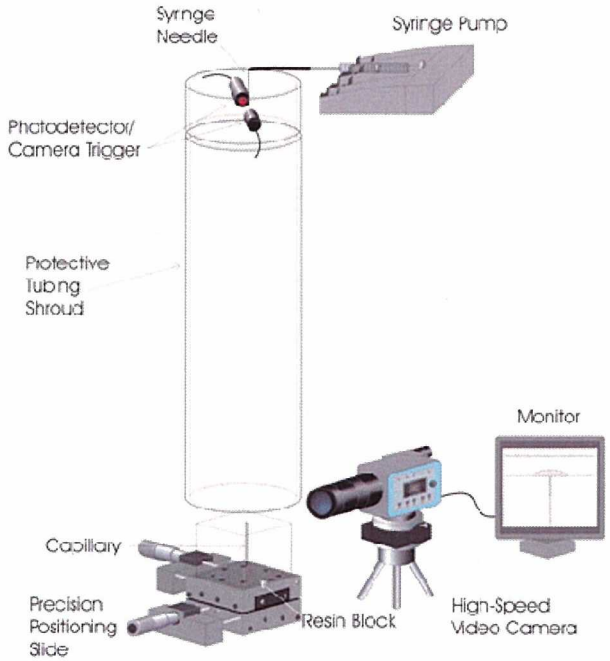

Figure 2. Schematic Diagram of Test Apparatus

In the falling droplet test system, droplets were generated using a syringe pump to feed liquid through a small needle at a flow rate of 0.03 mL/min, which was sufficiently low to eliminate any dynamic effects associated with the droplet formation and detachment processes and generate droplets with reproducible size. Experiments using deionized water and a 33 gauge needle (0.110 mm bore diameter) produced droplets of approximately 1.95 mm in diameter; an 18 gauge needle (0.838 mm bore diameter) produced droplets of approximately 3.44 mm in diameter.

The droplets were generated at the top of the test apparatus from where they fell under the influence of gravity, shielded from ambient air by a cylindrical shroud made of Plexiglas™, and impacted on a cast block containing the capillary. The test apparatus was designed to maintain the alignment of the droplet generation point and the target capillary, while allowing removal and replacement of the target block between tests for cleaning. Figure 3 shows the capillary block positioned on the droplet impact stage of the test system.

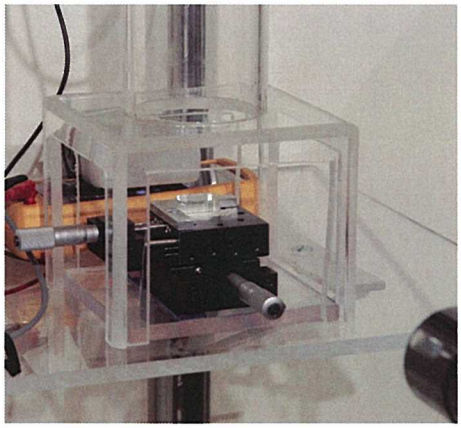

Figure 3. Photograph of the X-Y Stage and Capillary Block

The target capillary blocks were cast from a transparent epoxy resin (EPON® 815C, Shell Epoxy Resins, LLC, Houston, TX) to allow observation of the dynamics of liquid impact and flow through the capillary. Three capillary diameters were used in the experiments: 0.1 mm, 0.3 mm, and 0.5 mm. The impact events were recorded using a Phantom 7 (Vision Research, Inc., Wayne, NJ) high-speed video camera. The frame rate used for the capillary impact study was 26,000 frames per second (fps) at 256 x 256 pixel resolution (providing 23 μm/pixel spatial resolution and 38 μs temporal resolution). A 2 μs shutter speed was used to freeze droplet motion in each image. Image scale was determined by calibration of the field of view prior to the droplet impact experiments.

Since timing was critical for the video recordings, a photo detector was located below the needle tip, connected to the trigger circuit and a delay timer to start video recording as the droplet neared the impact surface. Two photographic flash units were used in tandem (Model 580 EX, Canon, USA) to illuminate the impact. The sequential flashes provided sufficient illumination to record 4 to 7 ms of an impact event. The diameter and impact velocity of the test droplet were determined from the video record of the droplet immediately before the impact, which was done using the Phantom 630A image analysis software. Figure 4 shows a test droplet as it approached the surface of a capillary block.

The tests were performed using deionized (DI) water and a 0.1 percent aqueous solution of surfactant Triton X-100 used

to reduce the surface tension of water from 0.072 N/m to approximately 0.03 N/m. Table 1 shows droplet diameters and impact velocities used in the tests.

Figure 4. Test Droplet Approaching Surface of a Capillary Block

Table 1. Test Droplet Diameters and Impact Velocities

	Needle Diameter			
	0.838 mm (18 gauge)		0.110 mm (33 gauge)	
	DI d_0=3.44mm	Triton d_0=2.64mm	DI d_0=1.95mm	Triton d_0=1.40mm
Height (m)	u (m/s)		u (m/s)	
0.29	2.33	2.13[a]	2.27	2.23
0.61	3.33	3.27	3.17	3.07
1.34	4.74	4.57	(b)	(b)
1.83	5.41	5.16	(b)	(b)

(a) The drop height was 0.25 m
(b) Not tested.

Figure 5 shows a sequence of frames from a representative impact of a droplet on the 0.5 mm capillary block. The spread and penetration fronts of the liquid can be seen clearly as the droplet contacts the surface, flattens and spreads over the block in a thin disk, and flows into the capillary. As the spreading slowed, the edge of the disk became irregular (not shown in this sequence of images), but did not break into secondary drops under the test conditions used in this work.

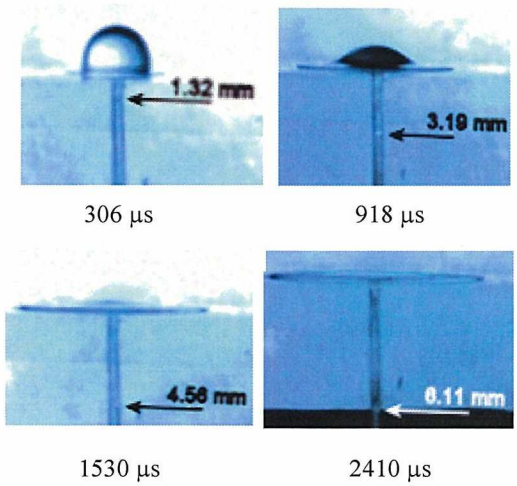

Figure 5. Impact of a 2.64 mm Droplet (0.1% Triton X-100 Solution) at 2.13 m/s Velocity on a 0.5 mm Capillary Block.

The penetration distance and spread radius were recorded from each video frame, an example of which is shown in Table 2. The velocity of the capillary flow was then calculated from the penetration distance data.

Table 2. Test Data for Impact of a 2.64 mm Droplet (0.1% Triton X-100 Solution) at 2.13 m/s Velocity on a 0.5 mm Capillary Block

Time After Impact (µs)	Penetration Distance (mm)	Spread Radius (mm)
115	0.32	1.05
153	0.68	1.14
191	0.86	1.50
229	1.00	1.68
306	1.32	1.96
344	1.40	2.10
574	2.17	2.73
612	2.46	2.82
880	3.03	3.32
918	3.19	3.46
1224	3.92	3.92
1300	4.02	4.01
1530	4.56	4.28
1836	5.20	4.55
2104	5.61	4.74
2410	6.11	4.87
3748	7.38	5.10
4093	7.52	5.10

STUDY RESULTS AND DISCUSSION

A total of 12 tests were performed in this work according to the test matrix shown in Table 1. For each of the tests, model calculations were performed as described in the Theoretical Analysis section of this paper. Figure 6 shows experimental data for the capillary meniscus penetration distance and velocity obtained in a representative test, which are shown using the circular and square symbols, respectively. The results of theoretical calculations performed using the Bosanquet equation (Eq.3) are also plotted in Figure 6 with the thin blue lines - solid line for the penetration distance and dashed line for the velocity. As illustrated in Figure 6 using an example test, model calculations were found to reflect the overall trends in the liquid penetration behavior reasonably well but to consistently under-predict the actual values of the penetration distance and velocity of liquid in the capillary, which was observed for all test conditions studied in this work.

As mentioned above, droplet impact pressure appears to be a dominant factor in developing the capillary flow of liquid in a droplet impact event. However, from the limited information published on this subject in the literature a great deal of uncertainty is associated with the pressure pulse profile that develops within the droplet upon impact. Therefore, Eq.(8) that calculates the initial impact pressure P_0 was investigated.

According to Eq.(8), the peak impact pressure was assumed to constitute 70% of the total kinetic energy of the falling droplet, but calculations using this factor result in under-predicting the rate of liquid penetration into the capillary in the droplet impact event. Moreover, increasing the pressure coefficient to 1.0 (i.e., all of the kinetic energy converted into the initial impact pressure) and neglecting any pressure decay during the droplet spread stage did not bring model predictions into agreement with the experiment.

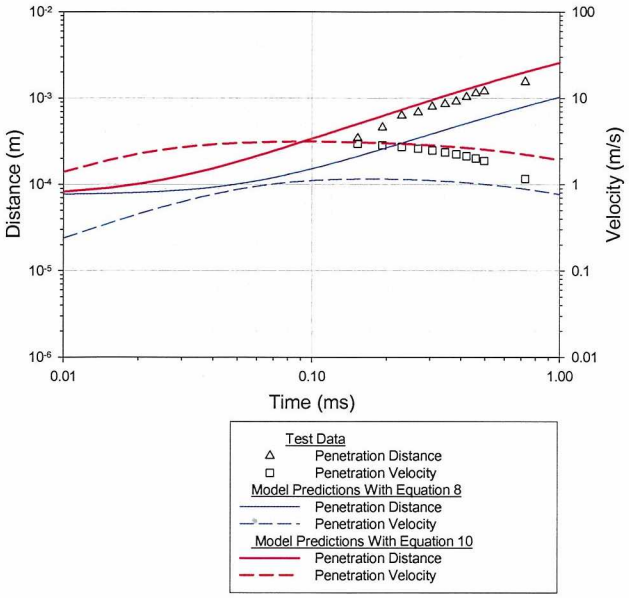

Figure 6. Comparison of Model Predictions and Test Data (1.40 mm Droplet Diameter, 0.1% Triton X-100, 2.23 m/s Fall Velocity, 0.3 mm Capillary)

One possible explanation for the discrepancy between test data and calculated results is that impact-induced shock waves that will develop in the droplet at the moment of impact may produce an amplified pressure pulse at the inlet to the capillary higher than the droplet-averaged pressure spike calculated by Eq.(8). In fact, a number of video recordings of the droplet impact events showed some distortions that occurred on the surface of the droplet during its spread on the capillary block. The additional pressure due to the shock reflection and amplification in the liquid will cause an increase in liquid penetration rate into the capillary.

In order to achieve better agreement between theoretical calculations and experimental results calculations were performed using a range of values for the pressure coefficient in Eq.(8) for each test. Then, for each test, an optimum value of the pressure coefficient was determined by visually comparing the corresponding model predictions with the experimental data. The optimum pressure coefficients, determined for each of the test impact velocities, were averaged for the three capillary diameters and plotted in Figure 7 using the symbols. A simple linear regression in the form of $Coef$=1.72+1.30·u was then obtained to relate the pressure coefficient to the droplet impact velocity, which is also shown in Figure 7 along with the 95% confidence interval for the regression. Using the droplet impact pressure–velocity correlation coefficient determined in this way, the following modification is suggested for Eq.(8) for the peak droplet impact pressure:

$$P_0 = (1.72+1.30u)\frac{\rho \cdot u^2}{2} \qquad (10)$$

It should be noted that Eq.(10) is based on the purely empirical basis, using a set of limited and scattered test data. Further research in the area of droplet impact pressure profile developing upon droplet impact on a capillary is recommended. Nevertheless, theoretical calculations performed using the modified Bosanquet equation [Eq.(3)] and Eq.(10) for the droplet impact peak pressure show good agreement with the experimental data obtained during testing. These adjusted model predictions are plotted in Figure 6 with the heavy red lines - solid line for the penetration distance and dashed line for the velocity, like before. Similar degree of agreement was achieved for most of the tests performed in this work, as shown in another example in Figure 8 plotted for the test results shown above in Table 2.

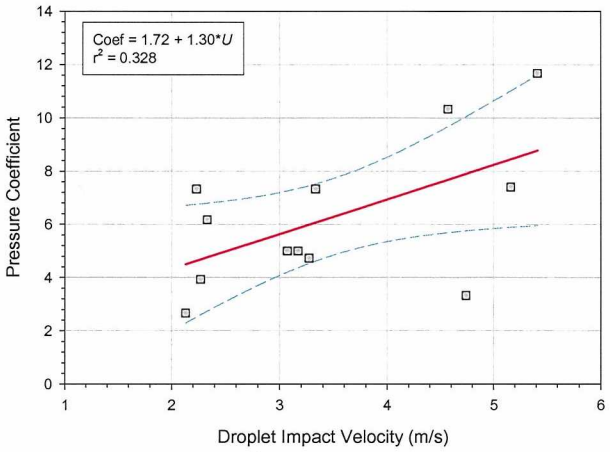

Figure 7. Droplet Impact Pressure – Velocity Correlation Coefficient

In addition to the comparison of theoretical predictions and experimental results obtained for the capillary flow, Figure 8 also shows a good agreement between test data and calculations for the dynamics of droplet spreading on the surface of the capillary block, which was calculated using Eq.(9).

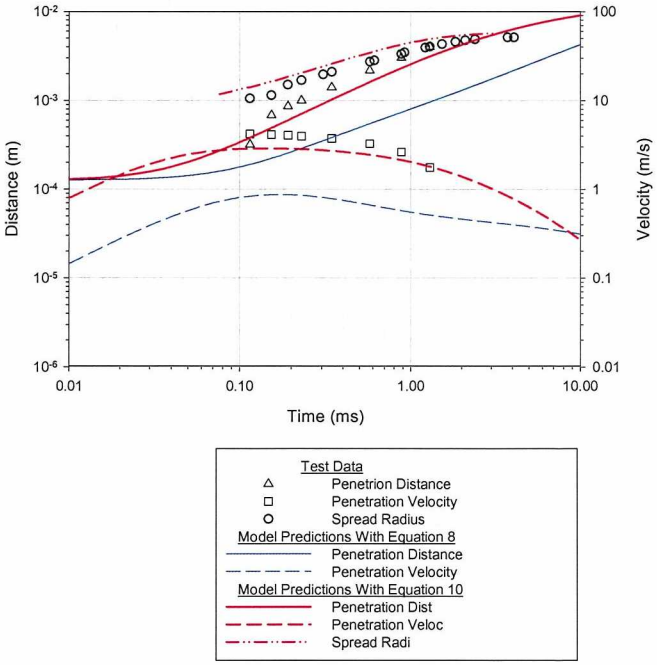

Figure 8. Test Results and Theoretical Calculations for Impact of a 2.64 mm Droplet (0.1% Triton X-100 Solution) at 2.13 m/s Velocity on a 0.5 mm Capillary Block

NOMENCLATURE

Symbol	Quantity	SI Unit
Coef	Pressure fit coefficient	Pa
d_{sf}	Final droplet spread diameter	m
d_0	Droplet fall diameter	m
g	Gravitational acceleration	m/s²
h_e	Current droplet height	m
k	Droplet spread time constant	1/s
P_e	Externally applied pressure	Pa
P_0	Initial impact pressure	Pa
r	Radial position of interest	m
r_c	Capillary radius	m
r_s	Current droplet spread radius	m
r_{sf}	Final spread radius	m
r_{s0}	Initial spread radius	m
Re	Reynolds Number	Dimensionless
t	Time since impact	s
t_{sf}	Final spread time	s
u	Impact velocity	m/s
We	Weber Number	Dimensionless
X	Fraction of final spread radius reached in final spread time	Dimensionless
z	Penetration depth	m
α	Radial pressure decay constant	Dimensionless
θ	Contact angle	radians
μ	Liquid viscosity	Pa-s
ρ	Liquid density	kg/m³
σ	Surface tension	N/m

REFERENCES

[1] R. Lucas, *Kolloid Zeitung,* vol. 23, p. 15, 1918.

[2] E. W. Washburn, The Dynamics of Capillary Flow. *Phys. Rev.*, pp. 273-283, 1921.

[3] B. V. Zhmud, F. Tiberg, and K. Hallstensson, Dynamics of Capillary Rise, *J. Colloid Interface Sci.*, vol. 228, pp. 263-269, 2000.

[4] C. H. Bosanquet, *Philosophical Magazine*, Serial 6 (45), pp. 525–531, 1923.

[5] B. L. Scheller and D. W. Bousfield, Newtonian Drop Impact with a Solid Surface, *AIChE J.*, vol. 41 (6), p. 1357, 1995.

[6] M. Toivakka, Numerical Investigation of Droplet Impact Spreading in Spray Coating of Paper, *Proc. Advanced Coating Fundamental Symposium*, May 11-15, Chicago, IL, 2003.

[7] T. Mao, D. Kuhn, and H. Tran, Spread and Rebound of Liquid Droplets upon Impact on Flat Surfaces, *AIChE J.*, vol. 43 (9), p. 2169, 1997.

[8] M. Pasandideh-Fard, Y. M. Qiao, S. Chandra, and J. Mostaghimi, Capillary Effects during Droplet Impact on a Solid Surface, *Phys. Fluids*, vol. 8 (3), p. 650, 1996.

[9] C. Ukiwe, Ali Mansouri, and D.Y. Kwok, The Dynamics of Impacting Water Droplets on Alkanethiol Self-Assembled Monolayers with Co-adsorbed CH_3 and CO_2H Terminal Groups, *J. Colloid Interface Sci.*, vol. 285, pp. 760-768, 2005.

[10] G. L. Chahine and K.M. Kalumuck, The Influence of Structural Deformation of Water Jet Impact Loading, *J. of Fluids and Structures*, vol. 12, pp. 103-121, 1998.